

Surface superconductivity in the topological Weyl semimetal t-PtBi₂

Sebastian Schimmel^{1,2,*}, Yanina Fasano^{2,3}, Sven Hoffmann^{1,2}, Julia Besproswanny^{1,2}, Laura Teresa Corredor Bohorquez², Joaquín Puig^{2,3}, Bat-Chen Elshalem⁴, Beena Kalisky⁴, Grigory Shimpunov^{2,†}, Danny Baumann², Saicharan Aswartham², Bernd Büchner^{2,5}, Christian Hess^{1,2,*}

¹ *Fakultät für Mathematik und Naturwissenschaften, Bergische Universität Wuppertal, 42097 Wuppertal, Germany*

² *Leibniz-Institute for Solid State and Materials Research (IFW-Dresden), Helmholtzstraße 20, 01069 Dresden, Germany*

³ *Instituto de Nanociencia y Nanotecnología and Instituto Balseiro, CNEA – CONICET and Universidad Nacional de Cuyo, Centro Atómico Bariloche, Avenida Bustillo 9500, 8400 Bariloche, Argentina*

⁴ *Bar Ilan University, Ramat Gan, 5920002, Israel*

⁵ *Institute of Solid State and Materials Physics and Würzburg-Dresden Cluster of Excellence ct.qmat, Technische Universität Dresden, 01062 Dresden, Germany*

**Corresponding authors*

†Present address: Institute of Physics, University of Amsterdam, 1098 XH Amsterdam, The Netherlands

Summary

The advancement of quantum computation is eager on generating fault tolerant qubits, and topological superconductivity is a very promising concept for reaching this goal¹⁻³. Early experimental achievements study hybrid systems⁴⁻⁵ as well as doped intrinsic topological or superconducting materials⁶⁻⁸ presenting the phenomena at very low temperatures. However, higher critical temperatures are indispensable for technological exploitation. Promising very

recent angle-resolved photoemission spectroscopy results reveal that superconductivity of the type-I Weyl semimetal trigonal PtBi₂ (t-PtBi₂) is located at the Fermi arcs surface states⁹ which renders t-PtBi₂ a candidate for intrinsic topological superconductivity. Here we show, using scanning tunnelling microscopy and spectroscopy (STM/STS) that t-PtBi₂ presents surface superconductivity at elevated temperatures (5 K). The gap magnitude is elusive: it is spatially inhomogeneous and spans from 0 to 20 meV. In particular, the large gap value and the shape of the quasiparticle excitation spectrum resemble the phenomenology of high- T_c superconductors. To our knowledge, this is the largest superconducting gap so far measured in a topological material. Moreover, we show that the superconducting state at 5 K persists up to 12 T magnetic field. Thus, we show that t-PtBi₂ is a prime candidate for intrinsic topological superconductivity at technologically relevant temperatures, fields and gap magnitudes.

The quest for materials presenting an interplay between superconductivity and topologically protected electronic surface states has sped up recently due to their exciting possibilities of application in emergent quantum technologies^{2-3, 10-19}. For instance, Majorana fermions are promising candidates for realizing quantum computation topologically protected from decoherence¹. These zero energy modes can be hosted by ferromagnetic atomic chains on a superconductor^{1,4,5}, topological quantum spin liquids²⁰⁻²², and topological materials with superconducting properties²³⁻²⁷. Among the latter, semimetals with linear dispersing bands have recently attracted the attention of the materials science community²⁸⁻²⁹. There are reports on the interplay of superconductivity and type-II Weyl semimetal behaviour in transition metal dichalcogenides^{14,17}. In Weyl semimetals strong spin-orbit coupling and broken time-reversal or inversion symmetry lift the degeneracy of the linear dispersive bands, a condition that might allow the establishment of topological superconductivity^{13,24}.

Very promising advances in finding an intrinsic topological superconductor suitable for technological applications have been made during the last year when studying the electronic properties of the van der Waals layered trigonal PtBi₂ (t-PtBi₂) compound. First, it was disclosed that this compound, while presenting the electronic structure of a type-I Weyl semimetal,¹⁰ is also a superconductor with a critical temperature of about 0.6-1.1 K according to transport measurements on bulk crystals^{30,31}. Second, transport experiments on flakes with thicknesses up to tens of nanometers reveal a Berezinskii-Kosterlitz-Thouless transition and thus provide strong evidence for two-dimensional superconductivity¹⁰. Third, published point contact spectroscopy data report a critical temperature $T_c \approx 3.5$ K³², while unpublished work points towards an even higher $T_c \approx 8$ K³³. Fourth, very recent angle-resolved photoemission spectroscopy (ARPES) measurements, in combination with band structure calculations, show that the topological Fermi arcs at the surface bear the superconducting properties of t-PtBi₂ up to about 10 K, whereas electronic states of the bulk are non-superconducting⁹. Yet another evidence of surface superconductivity is provided by scanning SQUID results which detect a sizeable diamagnetic signal at 6.4 K, characteristic of a 2D superconductor (see supplementary material). Thus, evidence for surface superconductivity of t-PtBi₂ is growing, and the connection of such a surface superconductivity with the predicted topological Weyl fermiology of this material¹⁰, renders it a promising candidate for intrinsic topological superconductivity.

Motivated by these findings, we use scanning tunnelling microscopy (STM/STS) to further explore the surface electronic structure of t-PtBi₂, and characterize the magnitude as well as the magnetic field and spatial dependence of the superconducting gap, i.e., crucial information for rationalising the nature of superconductivity in this compound. More specifically, we report on STM/STS data of t-PtBi₂ at 30 mK and at 5 K, and high magnetic fields up to 15 T.

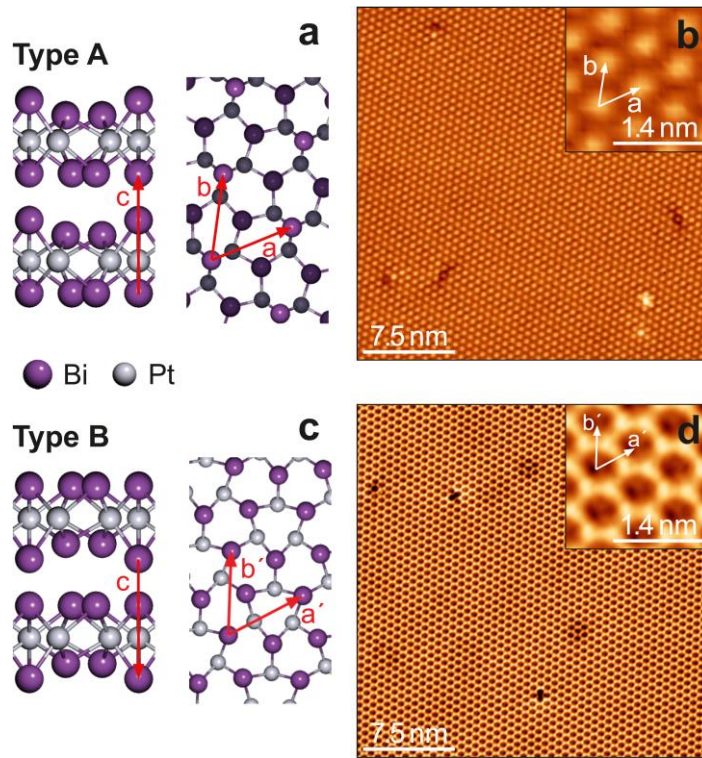


Figure 1: Crystal structure and STM topographies of non-centrosymmetric t-PtBi₂. (a) Schematics of the crystal structure with the sample terminating at a corrugated Bi plane (type A surface). Left: lateral view with the lattice parameter $c = 6.167 \text{ \AA}$ (Ref. 30) indicated. Right: Top view with the in-plane lattice parameters indicated, $a = b = 6.573 \text{ \AA}$ (Ref. 30). The topmost Bi atoms of the last layer are shown brighter. (b) Constant current topographic image of the typical atomic corrugation of a type A surface with bright spots arranged in a hexagonal lattice ($29 \times 29 \text{ nm}^2$, 400 pA and 350 mV). (c) Crystal structure in which the surface Bi atoms are in a coplanar arrangement (type B surface). Left: lateral view. Right: Top view with the in-plane lattice parameters indicated. (d) Constant current topographic image of the typical atomic corrugation observed on type B surface resembling a honeycomb structure ($29 \times 29 \text{ nm}^2$, 800 pA and 7.5 mV). Inserts: Zoom-ins of the main images with the unit cell vectors indicated. All measurements performed at $T = 30 \text{ mK}$.

Our topographic STM measurements on t-PtBi₂ (Fig. 1) reveal two types of cleaved surfaces, in agreement with a previous report³⁴. In this earlier work no signatures of superconductivity were reported. As is shown in the schematics of the crystal structure of Fig. 1, t-PtBi₂ is composed of layers stacked along the c -axis where coplanar Pt atoms are sandwiched in between two sheets of Bi atoms. In one sheet the Bi atoms are coplanar, too, but the other has a corrugation on the location of Bi atoms in the c -axis direction. These two types of Bi sheets are pairwise van der

Waals bonded, and the natural cleaving plane is thus in between these layers. We label the two different corrugated and flat Bi cleaved surfaces as type A and B, respectively.

Figure 2 shows the most important results of this work: The surfaces of t-PtBi₂ present a superconducting quasiparticle excitation spectrum with sizeable gap magnitude: The STM spectra are particle-hole symmetric with a depletion around zero bias and clear coherence peaks. This can be well recognized in Fig. 2 (a) which shows dI/dV_B zero magnetic field data, measured on a type B surface at $T = 5$ K. Note, that the zero bias conductance (ZBC) amounts to about 85% of the normal conductance. This clearly shows that only a fraction of the density of states (DOS) is gapped out by the superconducting state. Without further analysis, this observation is consistent with the presence of both superconducting surface states and normal bulk states which are simultaneously probed by the tunnelling tip. Note that the tunnelling signal is integrative with respect to the electronic wave vector k . Our interpretation therefore is also well consistent with ARPES data, where superconducting and normal states are observed for different regions in k -space⁹.

After having established the signatures of surface superconductivity in the tunnelling data, we address the magnetic field dependence: Figure 2 (b) shows a representative dI/dV_B spectrum measured at $B = 9$ T on the same cleaved surface, and Figure 2 (c) shows a systematic investigation of the superconducting DOS as a function of field up to $B = 15$ T. Up to 9 T no significant effect of the magnetic field is observable. However, upon increasing B to 12 T the coherence peaks fade away and the depletion in the low-energy conductance fills in, indicative of $B_{c2} \approx 12$ T which we interpret as a rough estimate of the orbital limiting field $B_{c2} = \Phi_0/2\pi\xi^2$. Remarkably, the resulting coherence length $\xi \approx 5$ nm is extremely short and, interestingly, it is 1-2 orders of magnitude smaller than values found in transport measurements¹⁰.

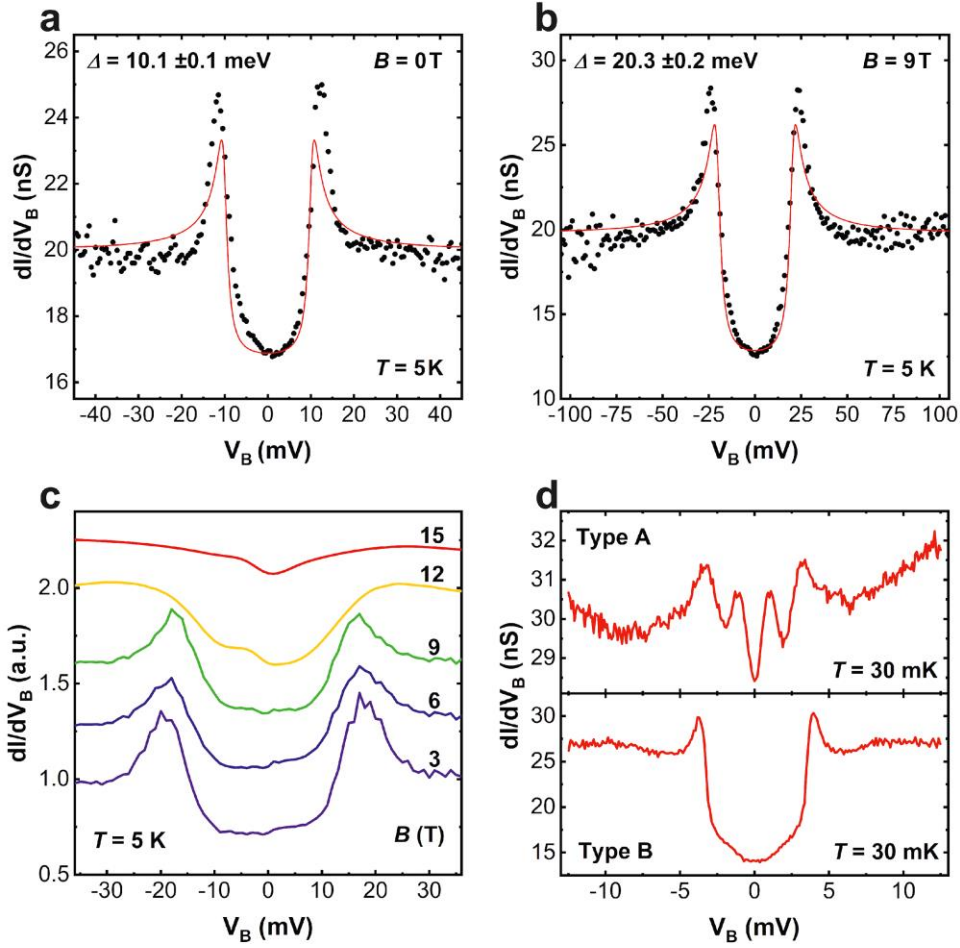


Figure 2: Superconducting gap of t-PtBi₂ and its closing with field. (a) Example of a dI/dV_B spectrum (black circles) measured at zero field in a type B surface (stabilisation conditions $V_B = 50$ mV, $I = 1$ nA). The red line is a fit to the data considering an s -wave BCS density of states with a Dynes quasiparticle lifetime shortening term plus a constant offset yielding a gap of $\Delta = 10.1 \pm 0.1$ meV, $\Gamma = 1.01 \pm 0.13$ meV, $C = 3.46 \pm 0.18$ nS, $D = 16.5 \pm 0.2$ nS, $R^2 = 0.801$. Note that the data leave room for multiple gap fitting or a nodal order parameter (see section Methods and Supplementary Information). However, we consider only the leading gap magnitude which is free of ambiguities. (b) STM spectrum measured at $B = 9$ T (stabilisation conditions: $V_B = 150$ mV, $I = 3$ nA) in a particular region of the same sample where we observed the maximum superconducting gap of $\Delta = 20.3 \pm 0.2$ meV, $\Gamma = 2.44 \pm 0.23$ meV, $C = 7.85 \pm 0.16$ nS, $D = 11.9 \pm 0.3$ nS, $R^2 = 0.835$. (c) Evolution of the quasiparticle excitation spectrum (normalized tunnel conductance) with the applied field, acquired in the same cleaved surface (stabilisation conditions: $B = 3, 9, 12, 15$ T, $V_B = 150$ mV, $I = 3$ nA; $B = 6$ T, $V_B = 100$ mV, $I = 2$ nA). (d) dI/dV spectra measured on two samples of opposite surface type exhibiting a smaller superconducting gap (stabilisation conditions: $V_B = 25$ (15) mV, $I = 0.8$ (0.4) nA, $V_{\text{mod}} = 200$ (150) μ V, $f_{\text{mod}} = 667$ (667) Hz for type A (type B) surface).

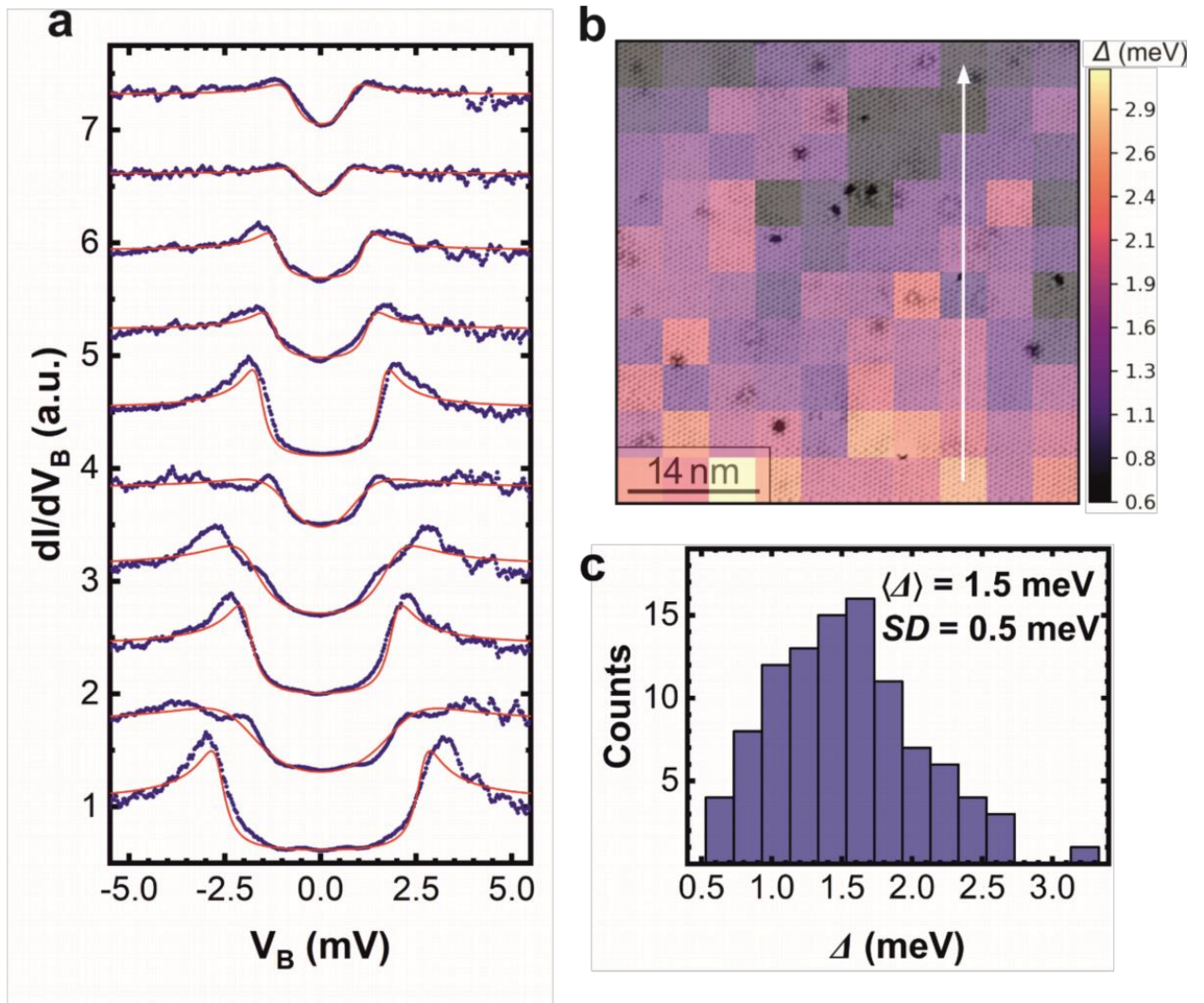


Figure 3: Spatial inhomogeneity of the superconducting gap for a type B atomically flat terrace of t-PtBi₂ measured at zero field. (a) Trace of ten normalized dI/dV_B curves out of a 10 x 10 grid covering an area of 50 x 50 nm². The experimental data are shown with blue circles whereas red lines correspond to fits to the data with an s-wave BCS density of states considering a Dynes quasiparticles' lifetime shortening term and a constant offset. (b) Map of the local value of the superconducting gap obtained from the fits. The vertical white arrow indicates the location where the trace of spectra of panel (a) was acquired. (c) Histogram of the superconducting gap values shown in (b) indicating the mean $\langle \Delta \rangle$ and geometrical standard deviation SD values. The measurements were performed at 30 mK in sample #10 with regulation conditions 1.5 nA and 15 mV.

In order to quantify the gap magnitude Δ in the tunnelling data, we fit the data with the BCS density of states of an s-wave superconductor plus a constant offset with the latter accounting for the residual non-superconducting DOS. For the zero field data in Fig. 2 (a) we obtain a large $\Delta = 10.1 \pm 0.1$ meV. We mention that alternative nodal or multi-gap order parameters yield similar

results for the leading gap (see Methods). Note that such a gap magnitude is comparable to that found in cuprate high- T_c superconductors³⁵, suggestive of a critical temperature significantly higher than our measurement temperature: A simple estimate using the weak coupling BCS ratio yields $T_c = \Delta / 1.764 k_B \approx 66$ K. A large gap magnitude is as well found for the data in magnetic field up to 9 T (panels (b) and (c) of Fig.1). Remarkably, the gap magnitude is significantly larger (a BCS fit to the 9 T-data (panel b) yields $\Delta = 20.3 \pm 0.2$ meV). While we cannot *a priori* exclude that the gap magnitude generally increases in moderate magnetic field, we suggest that the seemingly increased gap magnitude in magnetic field is rather the indication of a spatial inhomogeneity of superconductivity, even if measured on the same surface.³⁶ Interestingly, this notion is supported by further experiments on different surfaces of t-PtBi₂ which yield a large variability of the gap ranging from complete absence of superconductivity over relatively small $\Delta = 1-3$ meV to the just discussed very large $\Delta = 10-20$ meV, see Fig. 1 (d) and Extended Data Fig. 1.

In order to further address the apparent spatial variability of the superconducting gap at the local scale, we show in Fig. 3 (b) a gap map of the type B surface of sample #10 covering a 50×50 nm² field of view. Clearly, the values of the gap range from 0.5 to 3 meV, i.e., there is clear-cut evidence of the spatial inhomogeneity of superconductivity at the nanoscale. Note, that there is no apparent correlation between the gap magnitude and the location of surface defects (see panel (b) of Fig. 3). Note further, that the observed local-scale inhomogeneity in real space points to an interesting connection with ultra-sharp spectral features in ARPES data⁹: While on average, the real space data in Fig. 3 agree with the ARPES gap magnitude, one might conjecture that the large spatial inhomogeneity of the former and the sharpness in the \mathbf{k} -resolved data of the latter are uncertainty-related or connected to the different time scales of the STM and ARPES experiments. The actual origin of the spatial inhomogeneity remains unclear. We speculate that a strong 2D nature of superconductivity might foster spatial and/or temporal fluctuations of the order parameter. Furthermore, the impact of surface boundaries (e.g. step edges) and interlayer coupling in t-

PtBi₂ which is prone to exfoliation remains to be investigated, in particular if the surface superconductivity eventually will be revealed as being truly topological. The 2D and fluctuating character of superconductivity might also play an important role in the experimental fact that, despite all our efforts, we were not able to image vortices (see Extended Data Fig. 2). In this situation, theoretical work suggests divergent vortex displacement fluctuations³⁶. Further investigation is necessary to address all these intriguing aspects.

Before we conclude, we mention that the surface superconductivity observed at 5 K implies a new interpretation of the electrical transport data^{10, 30, 31}, where a transport $T_c = 0.6 - 1.1$ K is reported. More specifically, the transport T_c should not be understood as a true bulk T_c but rather as a result from the establishment of a percolative superconducting path which emerges from an ensemble of surface-superconducting layers in a crystal. This notion is supported by low-temperature specific heat data (see supplementary material) and magnetization data³¹, which reveal the absence of any bulk signature of superconductivity.

In conclusion, we investigate the surface superconductivity of t-PtBi₂ at elevated temperatures (~5 K). We observe surprisingly large gap values in the range of about 2-20 meV, suggesting a T_c that considerably exceeds the measurement temperature of 5 K. While the surface superconductivity exhibits spatial inhomogeneity, it is robust against out of plane fields up to about 12 T. The apparent large energy scale of the surface superconductivity not only implies a huge potential of t-PtBi₂ and related compounds for technological applications. It also challenges the theoretical understanding of the superconducting origin as well as material science approaches for controlling and enhancing the superconducting properties.

References

1. Kitaev, A. Yu. Unpaired Majorana fermions in quantum wires. *Phys.-Usp.* **44** 131 (2001)
2. Alicea, J. New directions in the pursuit of Majorana fermions in solid state systems. *Rep. Prog. Phys.* **75**, 076501 (2012).

3. Beenaker, C. W. J. Search for Majorana fermions in Superconductors. *Annu. Rev. Condens. Matter Phys.* **4**, 113 (2013)
4. Nadj-Perge, S. *et al.* Observation of Majorana fermions in ferromagnetic atomic chains on a superconductor. *Science* **346**, 6209 (2014).
5. Crawford, D. *et al.* Majorana modes with side features in magnet-superconductor hybrid systems. *npj Quantum materials* **7**, 117 (2022).
6. Sato, M. & Ando, Y. Topological superconductors: a review. *Rep. Prog. Phys.* **80**, 076501 (2017)
7. Wang, D. *et al.* Evidence for Majorana bound states in an iron-based superconductor. *Science* **362**, 333 (2018)
8. Machida, T. *et al.* Zero-energy vortex bound state in the superconducting topological surface state of Fe(Se,Te). *Nat. Mater.* **18**, 811 (2019).
9. Kuibarov, A. *et al.*, Superconducting Arcs, *Nature* **626**, 294 (2024).
10. Veyrat, A. *et al.* Berezinskii-Kosterlitz-Thoules Transition in the Type-I Weyl Semimetal PtBi₂. *ACS Nano Lett.* **23**, 1229 (2023)
11. Cho, G. Y., Bardarson, J. H., Lu, Y.-M., & Moore, J. E. Superconductivity of doped Weyl semimetals: Finite-momentum pairing and electronic analog of the ³He-A phase. *Phys. Rev. B* **86**, 214514 (2012).
12. Wei, H., Chao, S. -P., & Aji, V. Odd-parity superconductivity in Weyl semimetals. *Phys. Rev. B* **89**, 014506 (2014).
13. Hosur, P., Dai, X., Fang, Z., & Qi, X. -L. Time-reversal-invariant topological superconductivity in doped Weyl semimetals. *Phys. Rev. B* **90**, 045130 (2014).
14. Qi, Y. *et al.* Superconductivity in Weyl semimetal candidate MoTe₂. *Nature Comm.* **7**, 11038 (2016).
15. Bachmann, M. *et al.* Inducing superconductivity in Weyl semimetal microstructures by selective ion sputtering. *Sci. Adv.* **3**, e1602983 (2017).

16. Huang, C. *et al.* Inducing Strong Superconductivity in WTe_2 by a Proximity Effect. *ACS Nano* **12**, 7185 (2018).
17. Naidyuk, Y. *et al.* Surface superconductivity in the Weyl semimetal MoTe_2 detected by point contact spectroscopy. *2D Mater.* **5**, 045014 (2023).
18. Huang, C. *et al.* Proximity-induced surface superconductivity in Dirac semimetal Cd_3As_2 . *Nat. Comm.* **10**, 2217 (2019).
19. Dong W. -H. *et al.* Superconductivity and topological aspects of two-dimensional transition-metal monohalides. *npj Comput. Mater.* **8**, 185 (2022).
20. Kitaev, A. Anyons in an exactly solved model and beyond. *A. Ann. Phys.* **321**, 2 (2006).
21. Kasahara, Y. *et al.* Majorana quantization and half-integer thermal quantum Hall effect in a Kitaev spin liquid. *Nature* **559**, 227 (2018)
22. Wolter, A. U. B. & Hess, C. Spin liquid evidence at the edge and in bulk. *Nat. Phys.* **18**, 370 (2022).
23. Fu, L. & Kane, C. L. Superconducting Proximity Effect and Majorana Fermions at the Surface of a Topological Insulator. *Phys. Rev. Lett.* **100**, 096407 (2008).
24. Meng, T. & Balents, L. Weyl superconductors. *Phys. Rev. B* **86**, 54504 (2012).
25. Li, Y & Haldane, F. D. M. Topological Nodal Cooper Pairing in Doped Weyl Metals, *Phys. Rev. Lett.* **120**, 067003 (2018).
26. Yuan, Y. *et al.* Evidence of anisotropic Majorana bound states in 2M-WS_2 . *Nat. Phys.* **15**, 1046 (2019).
27. Yan, Z., Wu, Z., & Huang, W. Vortex End Majorana Zero Modes in Superconducting Dirac and Weyl Semimetals. *Phys Rev Lett.* **124**, 257001 (2020).
28. Kopnin, N. B., Heikkilä, T. T., & Volovik, G. E. High-temperature surface superconductivity in topological flat-band systems. *Phys. Rev. B* **83**, 220503 (2011).
29. Sharma, M. M., Sharma, P., Karn, N. K., & Awana, V. P. S. Comprehensive review on topological superconducting materials and interfaces. *Supercond. Sci. Technol.* **35**, 083003 (2022).

30. Shipunov, G. *et al.* Polymorphic PtBi₂: Growth, structure, and superconducting properties. *Phys. Rev. Materials* **4**, 124202 (2020).
31. Zabala, J. *et al.* Enhanced weak superconductivity in trigonal γ -PtBi₂, *J. Phys.: Condens. Matter* **36**, 285701 (2024)
32. Bashlakov, D. L., Kvitnitskaya O. E., Shipunov, G., Aswartham, S., Feya, O. D., Efremov, D. V., Büchner, B., Naidyuk Yu. G., Electron-phonon interaction and point contact enhanced superconductivity in trigonal PtBi₂. *Low Temp. Phys.* **48** 747 (2022)
33. Kvitnitskaya, O. *et al.*, unpublished data.
34. Nie, X. -A. *et al.* Robust Hot Electron and Multipole Topological Insulator States in PtBi₂. *ACS Nano* **14**, 2366 (2020).
35. Fischer, Ø., Kugler, M., Maggio-Aprile, I., Berthod, Ch., & Renner, Ch. Scanning tunneling spectroscopy of high-temperature superconductors. *Rev. Mod. Phys.* **79**, 353 (2007).
36. We mention, that for technical reasons the set of spectra in applied magnetic field (panels (b,c) of Fig. 2) were measured in a different location of the sample than the zero field data presented in Fig. 2 (a).
37. Vinokur, V.M. *et al.* Flux pinning and creep in very anisotropic high temperature superconductors, *Physica C* **168**, 29 (1990).

Methods

Crystal growth and characterisation

We studied ten samples of single crystalline t-PtBi₂ grown by means of the self-flux method as described in Ref. 30. The composition and crystal structure of the samples were determined by energy-dispersive x-ray spectroscopy and x-ray diffraction, respectively. In-plane resistivity was measured applying the four-probe method as a function of temperature in the ranges 0.1 – 300 K

using ^4He and dilution cryostats. Evidence of superconductivity has been found below 600 mK (Ref. 30).

Specific-heat measurements were performed on a single crystal between 0.4 and 10 K using a heat-pulse relaxation method in a Physical Properties Measurement System (PPMS, Quantum Design), in magnetic fields up to 1 T perpendicular to the ab plane. In order to obtain the specific heat, the temperature- and field-dependent addenda were thoroughly subtracted from the measured specific-heat values in the sample measurements.

STM setups

The measurements were carried out in two home-built low-temperature scanning tunneling microscope setups³⁸ with Nanonis SPM control systems³⁹. Mechanically sharpened PtIr tips served as the ground electrode. Data measured at $T = 5$ K was acquired by a liquid-helium-cooled scanning tunneling microscope with an energy resolution of about 2 meV (Ref. 38). Equipped with a superconducting magnet, this system allows us to execute field-dependent studies up to $B = 15$ T. We also used a second setup where the STM is attached to a dilution refrigerator yielding measurement temperatures down to 30 mK. This system has an improved energy resolution in the sub-meV regime. In order to prepare pristine atomically clean surfaces prior to the measurements, the platelet-like samples were cleaved in both devices at $T \sim 5$ K in cryogenic ultra-high vacuum atmosphere.

Data acquisition and analysis

Standard STM measurement techniques like the constant current and the $I(V_B)$ spectroscopy modes were applied to acquire the topographic and spectroscopic data, respectively. The dI/dV_B spectra were obtained by numerical differentiation of the $I(V_B)$ curves or via the commonly used lock-in technique - if used, indicated by the modulation parameters V_{mod} and f_{mod} . The data were analysed using the software for scanning probe microscopy WSxM⁴⁰.

In addition, in order to estimate the value of the superconducting gap we wrote a fitting program in Python language. The spectra were fitted using an s-wave BCS density of states, the Dynes parameter Γ (Ref. 41), and an additional constant D accounting for the contribution of a non-superconducting background:

$$dI/dV_B(V_B) = C |\operatorname{Re}\{(eV_B - i\Gamma)/[(eV_B - i\Gamma)^2 - \Delta^2]^{1/2}\}| + D$$

In the formula C is a proportionality constant, e denotes the charge of an electron and Δ is the superconducting gap. The broadening of spectroscopic features due to a finite quasiparticle lifetime is taken into account by the phenomenological Dynes parameter Γ . Upon fitting the data we also tested fits with a double s -wave order parameter, as well as with a nodal order parameter, where for the latter the k -dependent contribution of the gap to the differential conductance is of the form:

$$dI/dV_B(V_B)_k = C |\operatorname{Re}\{(eV_B - i\Gamma)/[(eV_B - i\Gamma)^2 - \Delta_k^2]^{1/2}\}| + D, \text{ where } \Delta_k = \Delta_0 \sin(\theta_k).$$

Measurements in magnetic field

The magnetic field dependence of the superconducting state was systematically studied after a zero-field cooling process: The samples were cooled down to ~ 5 K and then the field was applied. We measured increasing the field in steps $B = 3, 6, 9$ T, and then the field was set to the maximum available field of 15 T at which the superconducting gap was suppressed. Afterwards, the field was reduced to 12 T at which the superconducting gap was observed in the spectrum again. In order to guarantee the comparability of the spectra, throughout these investigations the tunnelling junction stabilisation resistance was kept constant at 50 M Ω .

Data availability

The data supporting the findings of this study are available from the corresponding author upon reasonable request. Source data are provided with this paper.

38. Schlegel, R. *Et al.* Design and properties of a cryogenic dip-stick scanning tunneling microscope with capacitive coarse approach control. *Rev. Sci. Instrum.* **85**, 013706 (2014).

39. SPECS Surface Nano Analysis GmbH, Voltastrasse 5 13355 Berlin / Germany, webpage: <https://www.specs-group.com/nanonis/products/> (2016).

40. Horcas, I. *et al.* WSXM: A software for scanning probe microscopy and a tool for nanotechnology. *Rev. Sci. Instrum.* **78**, 013705 (2007).

41. Dynes, R. C., Narayanamurti, V., Garno, J.P. Direct Measurement of Quasiparticle-Lifetime Broadening in a Strong-Coupled Superconductor *Phys. Rev. Lett.* **41**, 1509 (2007).

Acknowledgements

Work supported by the European Research Council (ERC) under the European Union's Horizon 2020 research and innovation programme (Grant Agreement No. 647276-MARS-ERC-2014-CoG) and by the Deutsche Forschungsgemeinschaft (DFG, German Research Foundation) Grants 500507880 and AS 523/4–1. Y.F. acknowledges support from the Georg Forster Research Prize from the Alexander von Humboldt Foundation. L.T.C. is funded by the DFG (project-id 456950766).

Author Contributions

C.H, S.S., and B.B. designed the research, S.S., S.H., J.P., Y.F., J.B., and D.B. performed STM measurements, L.T.C.B. conducted specific heat measurements, B.-C. E. and B.K. performed scanning SQUID measurements, G.S. and S.A. grew samples, S.S., S.H., J.P., and Y.F. analysed

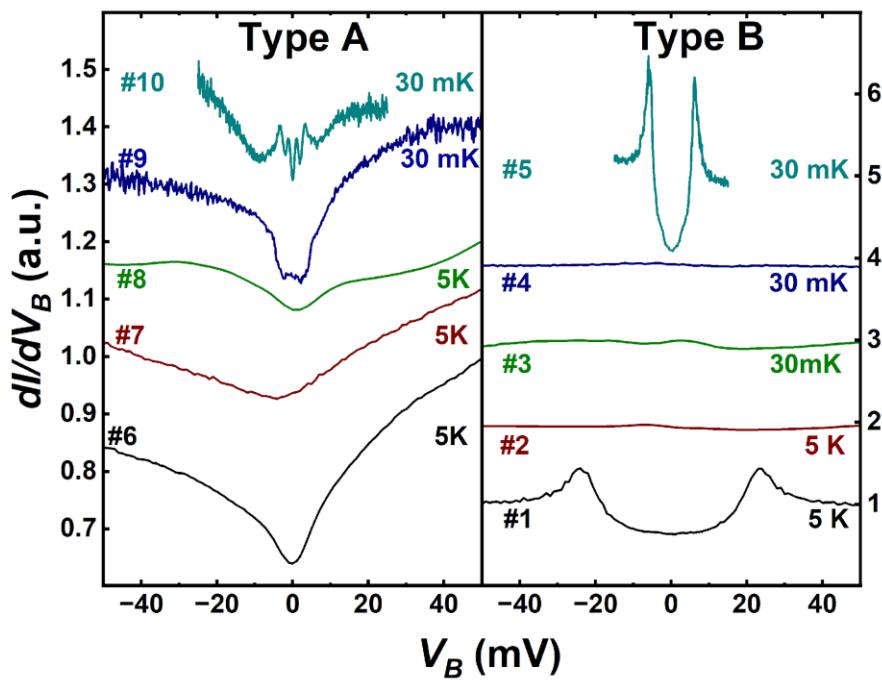
data; all authors discussed the data analysis and interpretation; S.S., Y.F., J.P., and C.H. wrote the paper.

Competing interests

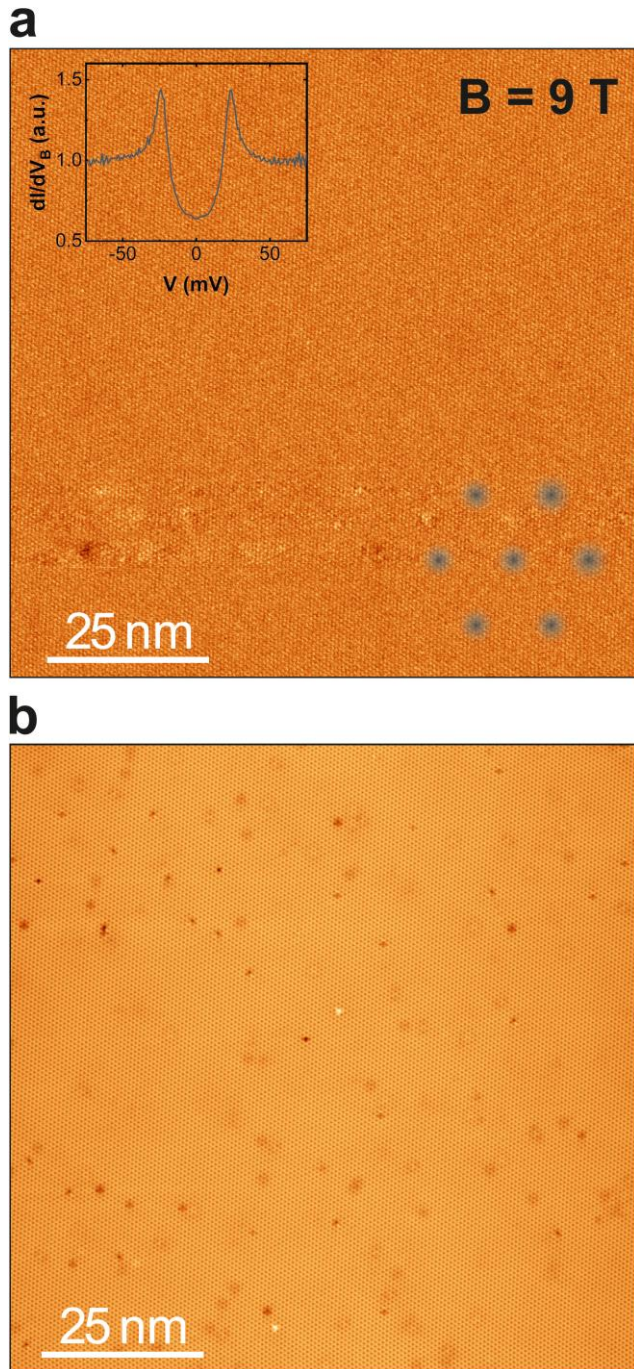
The authors declare no competing interests.

Correspondence and requests for materials should be addressed to Sebastian Schimmel and Christian Hess.

Extended data



Extended Data Figure 1: Typical normalized tunnel conductance spectra measured in the 10 t-PtBi₂ samples studied. Left panel: Data in type A surface. Right panel: Data in type B surfaces. Spectra have been shifted vertically for clarity. Measurements performed at 5 and 0.03 K.



Extended Data Figure 2: (a) Typical zero bias conductance map measured at 9 T and 5K in the type B surface of t-PtBi₂ sample #1. No signatures of local variations of conductance as expected when nucleating three dimensional vortices are observed even though the map registers the atomic corrugation. Top left insert: Typical tunnel conductance spectra acquired in the region where the zero bias conductance map was measured. Bottom right insert: Schematics of the three dimensional vortex structure expected for 9T with a lattice spacing of 16 nm. (b) Simultaneously acquired atomic-resolution topography of the region measured in panel (a). Stabilisation conditions were 100 pA and 1.2 mV.